molecules

MDPI

Article

Stable Zinc-Based Metal-Organic Framework Photocatalyst for Effective Visible-Light-Driven Hydrogen Production

Li-Long Dang [1,3], Ting-Ting Zhang [1,2], Ting-Ting Li [1], Tian Chen [1], Ying Zhao [1], Chen-Chen Zhao [1] and Lu-Fang Ma [1,*]

[1] Henan Province Function-Oriented Porous Materials Key Laboratory, College of Chemistry and Chemical Engineering, Luoyang Normal University, Luoyang 471934, China; danglilong8@163.com (L.-L.D.); zhangtingting131@126.com (T.-T.Z.); tingtinglichem@163.com (T.-T.L.); ctian2022@163.com (T.C.); zhaoyingchem@126.com (Y.Z.); chenchenzhao2022@163.com (C.-C.Z.)
[2] College of Materials and Chemical Engineering, China Three Gorges University, Yichang 443002, China
[3] Shanghai Key Laboratory of Molecular Catalysis and Innovative Materials, Fudan University, Shanghai 200438, China
* Correspondence: mazhuxp@126.com

Abstract: Herein, a new Zn-MOF material, [Zn(**L1**)(**L2**)], **1**, was built successfully through a one-pot solvothermal method. The 3D MOF structure was determined by Single X-ray diffraction analysis, IR, and elemental analysis. A series of PXRD tests of **1** after being immersed in different solvents and pH solutions demonstrated the good stability of **1**. Interestingly, this material displayed high catalytic activity for the visible-light-driven hydrogen generation under the illumination of white LED in pure water or a mixture of DMF and H_2O without additional photosensitizers and cocatalysts. Besides, the studies also showed that the catalytic activity changed constantly as well as the solvent ratio adjustment of DMF and H_2O from 4:6 to 2:8. Additionally, the catalytic activity reached the best value (743 μmol g^{-1} h^{-1}) when the solvent ratio was 4:6. The heterogeneous nature and recyclability of the MOF catalyst, as well as several factors that affect the catalytic activity, were investigated and described in detail. Moreover, the photocatalytic mechanism for the hydrogen generation of **1** was also proposed based on the fluorescence spectra and UV-vis absorption.

Keywords: metal-organic framework; photocatalytic hydrogen generation; fluorescence emission

Citation: Dang, L.-L.; Zhang, T.-T.; Li, T.-T.; Chen, T.; Zhao, Y.; Zhao, C.-C.; Ma, L.-F. Stable Zinc-Based Metal-Organic Framework Photocatalyst for Effective Visible-Light-Driven Hydrogen Production. *Molecules* **2022**, *27*, 1917. https://doi.org/10.3390/molecules27061917

Academic Editor: Wei-Yin Sun

Received: 21 February 2022
Accepted: 11 March 2022
Published: 16 March 2022

1. Introduction

The relentless consumption of fossil fuels raises an urgent issue about how to develop new energy sources to fill the gap of existing energy shortage. In this context, scientists have focused their attention to hydrogen fuel because hydrogen can be produced by water decomposition [1–4]. Therefore, exploring a variety of materials to facilitate the decomposition of water to generate hydrogen has sparked a scientific boom. During last decade, great progress has been made on splitting water to generate hydrogen covering the catalyst type from the initial homogeneous catalysts to heterogeneous species [5–8], improvement of catalytic performance, and repeatability optimization of the catalysts. The heterogeneous catalysts are increasingly favored due to their convenient recoverability and strong repeatability [9–12], and include metallic oxide, MOFs, etc. [13,14]. Meanwhile, MOFs, as a kind of novel porous metal-organic framework material, due to their high specific surface area, large porosity, and good structural stability have shown wide application prospects in gas adsorption [15–17], sensors [18–20], magnetic [21–25] optical materials [26–32], and catalysts [33–36], etc. Additionally, the MOF materials have been utilized to perform photocatalytic hydrogen production [37–41] and carbon dioxide reduction reactions [42–45]. For example, Su reported a amine-functionalized Co(II)-MOF catalyst through a one-pot solvothermal method. The material showed good photocatalytic hydrogen evolution

activity (1102 μmol g^{-1} h^{-1}. In addition, the CO_2 reduction performance was also explored, in which -NH_2 was used for light absorption and cobalt-oxygen clusters as catalytic nodes [46]. Besides, Du synthesized Ni-MOF materials displaying high catalytic activity for visible-light-driven hydrogen production under the illumination of white LED or direct sunlight [47]. Additionally, the heterogeneous nature and recyclability of the catalyst were studied carefully.

The research about MOF catalysts for hydrogen generation has made tremendous advances, including utilizing some organic ligands containing photosensitive groups, such as -NH_2- and so on. To our knowledge, the MOFs catalytic splitting decomposition of water into hydrogen generally consists of three parts: a photosensitizer, co-catalyst, and sacrificial agent. In general, the photosensitizer and co-catalyst are mainly composed of a platinum complex, which usually costs a lot [48–50]. Therefore, developing a new class of MOFs material that does not need additional photosensitizers and co-catalysts under the catalytic hydrolysis process of hydrogen production is of great significance.

Here, two organic ligands, 4, 4′-bibenzoic acid-2, 2′-sulfone (**L1**), 4, 4′-azopyridine (**L2**), were selected to build a new Zn-based metal-organic framework by coordinating with divalent zinc ion in a 1:1:1 ratio (Scheme 1). Finally, a new 3D MOF was obtained successfully in a high yield (63.5%), which was characterized by single-crystal X-ray diffraction, PXRD, IR, and elemental analysis, etc. Meanwhile, the PXRD tests after 1 was immersed in various solvents and pH conditions also reflected good solvent and pH stability of 1. Besides, the material showed high photocatalytic hydrogen production properties in pure water under the absence of the cocatalyst and photosensitizer. Furthermore, a comparative study of distinct solvent conditions, such as H_2O and DMF/H_2O in different ratios, displayed that the photocatalytic hydrogen generation properties reached their maximum when the ratio of DMF and H_2O was 4:6. Additionally, the recyclability of the catalyst, as well as factors that affect the catalytic activity were investigated and described in detail.

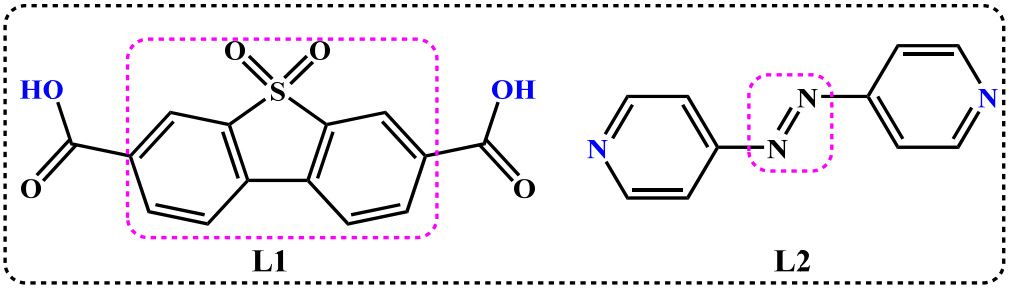

Scheme 1. Chemical structures of 4, 4′-bibenzoic acid-2, 2′-sulfone (**L1**) and 4, 4′-azopyridine (**L2**) in this work.

2. Results

2.1. The Structure of Complex **1**

The Zn (II) site in **1** was six-coordinated by four carboxylic oxygen atoms from three **L1** ligands, together with two nitrogen atoms belonging to two same **L2** ligands. Thereinto, the two carboxylic acid groups of **L1** ligand were coordinated by different coordination modes, viz., chelating coordination and monotone coordination form, to link three zinc ions. In organic ligand **L2**, the azo bonds existed in a stable *trans* configuration. The bond lengths were Zn1-O3 = 2.006 (2) Å, Zn1-O4 = 2.169 (2) Å, Zn1-O5 = 2.357 (3) Å, Zn1-O6 = 2.070 (2) Å, Zn1-N1 = 2.112 (3) Å, and Zn1-N4 = 2.194 (3) Å (Figure 1a). The adjacent Zn···Zn distances bridged by **L1** and **L2** were 5.068 and 13.224 Å, respectively. Interestingly, there existed obvious π···π stacking interaction between the opposite **L1** ligands (3.51 Å). Therefore, the coordination mode of Zn^{2+} ions and accumulation effect resulted in the formation of a three-dimensional (3D) framework (Figure 1).

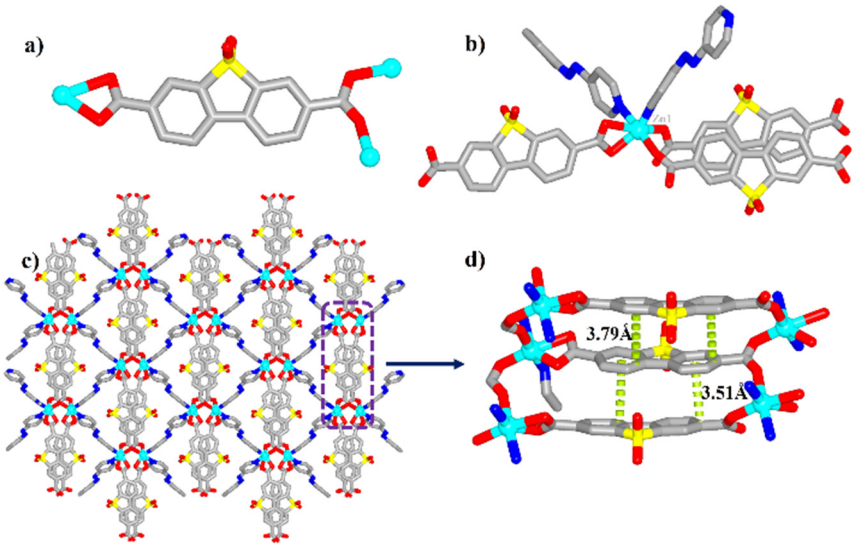

Figure 1. Single-crystal X-ray structure of **1**. Coordination geometry of ligand **L1** (**a**); coordination environment of Zn^{2+} ions in **1** (**b**); view of the 3D framework of **1** (**c**); view of π···π stacking interaction (3.79 Å and 3.51 Å) between **L1** ligands (**d**).

2.2. The TGA and Stability Exploration of **1**

Elemental analysis (EA), thermogravimetric (TG) analysis, Fourier transform infrared (FT-IR) spectrum, and powder X-ray diffraction (PXRD) were performed to characterize MOF complex **1**. The TG curve showed that the initial 3.5% weight loss of **1** happened at 150–360 °C, which should be ascribed to the loss of a small number of free water and DMF molecules. Then, a large weight loss (67.4%) could be observed from 360 to 485 °C, which was consistent with the weight of ligand **L1** (calcd. 67.6%), reflecting the decomposition of the skeleton of compound **1** and the loss of **L1**. After that, the residual components of **1** were gradually lost and eventually converted to zinc oxides, nitrides, and sulfides. This result is consistent with those of EA and crystal data (Figure 2). In addition, the IR spectrum of complex **1** exhibited a strong band at 1180 cm^{-1} owing to the C-N stretching vibrations and strong absorptions at 1592 cm^{-1} and 1302 cm^{-1} due to stretch of the C=O and C-O bonds from the carboxylate group of **L1** (Figure 2b). Moreover, the sharp strong absorptions at 1424 cm^{-1} and 1379 cm^{-1} are attributable to the stretching vibrations of N=N and C=S bonds. Additionally, the C-H bond absorption peaks of the pyridine group in **L2** could be observed at 3067 cm^{-1}.

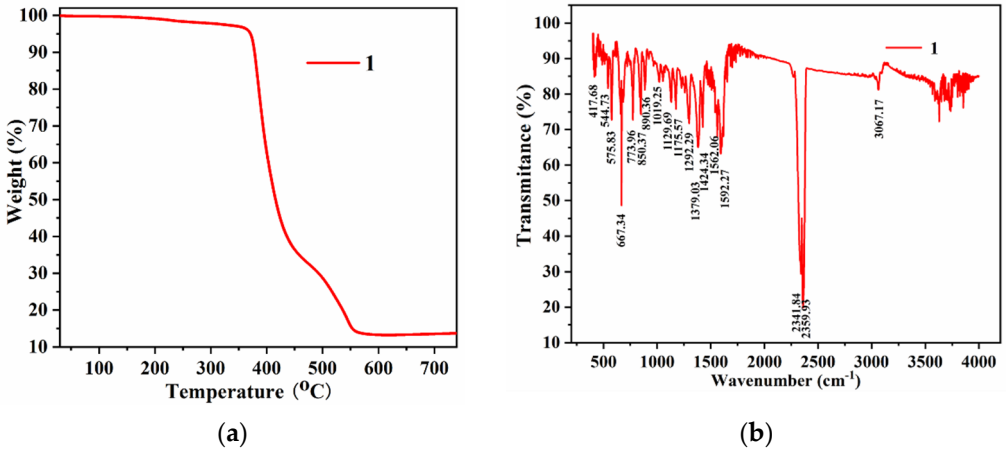

(**a**) (**b**)

Figure 2. Thermogravimetric analysis curve of **1** (**a**); IR spectrum of complex **1** (**b**).

In addition, the PXRD pattern showed that the diffraction peaks of as-synthesized Zn-MOF matched well with the simulated one in spite of the difference in peak intensity, suggesting the as-synthesized sample was single phase. Besides, a wider range of structural stability is significant for the study of the properties of the material in different conditions. Therefore, these samples were immersed in different solvents, such as CH_3CN, EtOH, MeOH, Dioxane, DMSO, $CHCl_3$, and so on for 3 days. Meanwhile, other samples were soaked in different pH solvents (range from 3–12). After that, the PXRD tests were carried out. The result displayed the PXRD matching was consistent between these samples and simulated data. Besides, the Zn leaching after being soaked in different pH solutions (pH = 3, 4, 6, 8, 10, 12) for 3 days was confirmed to be 63.84%, 60.46%, 4.72%, 4.86%, 5.28%, and 44.37% by inductively coupled plasma optical emission spectrometry (ICP-OES). The high Zn leaching reflected that the structures of complexes **1** in pH 3, 4, and 12 solution were destroyed. Additionally, the low Zn leaching value reflected the good stability of complexes **1** in the solutions (pH = 6, 8, 10) (Figure 3a). The results suggested good solvents and pH stability (range from 6–10) of **1**.

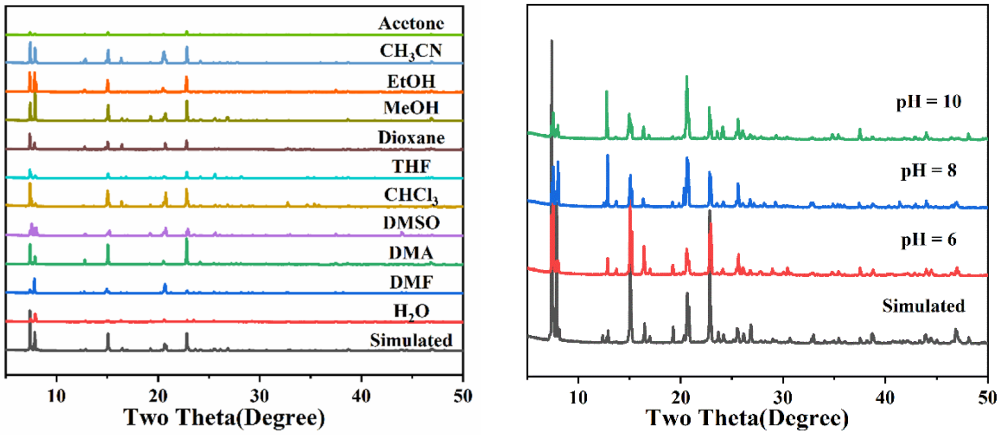

Figure 3. PXRD patterns of simulated (black) and after being immersed samples in different solvents of **1** (**a**); PXRD patterns of simulated (black) and after being immersed samples under different pH conditions of **1** (**b**).

2.3. The UV-Vis Absorption and Fluorescence Emission Spectra

To characterize the optical properties of MOF **1**, the solid-state UV-vis absorption spectra of ligands **L1** and **L2**, and **1** were measured and compared under ambient conditions. The results clearly showed that ligand **L2** displayed a broad absorption ranging from 250 to 500 nm. While, the complex also displayed a stronger and broader absorption under same variation range (from 250 to 550 nm). However, the pristine **L1** only exhibited sharp absorption ranging from 250 to 350 nm (Figure 4a). Therefore, compared with the pristine ligand **L1** and **L2**, the adsorption bands of **1** exhibited a significant red-shift. These properties are likely related to the effect of coordinated Zn (II) ions on the excited state of the ligand, d-d transitions of Zn (II) ions, and $\pi\cdots\pi^*$ stacking interaction of between **L1** ligands [51,52]. Besides, the Kubelka–Munk representation of **1** was also studied (Figure 4a). The band-gap energy (Eg) of **1** determined from Tauc's plot was 1.96 eV (Figure S7). The result reflected that **1** could be taken into account as ideal semiconductive MOFs and that such low energy values are infrequent for the MOF-series materials [53,54]. The result was very meaningful for photocatalytic hydrolysis to produce hydrogen because the valence band absorbs light energy to excite electrons into the conduction band, resulting in the production of light electrons. The electrons could be used to reduce water to produce hydrogen.

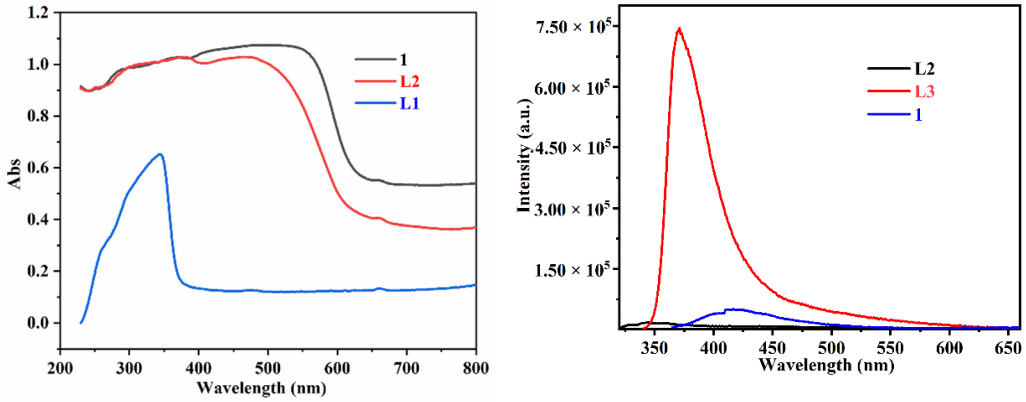

(**a**) (**b**)

Figure 4. Solid-state UV-Vis absorption; (**a**) emission spectra (**b**) of **L1**, **L2**, and **1**.

Meanwhile, the solid-state fluorescence emission spectra of ligands **L1** and **L2** and compound **1** were also explored carefully by the steady-state transient fluorescence spectrometer. By observing the data carefully, ligand **L1** showed very strong blue fluorescence emission at 375 nm when excited at 307 nm. However, an extremely weak blue fluorescence emission at 350 nm could be observed for ligand **L2** when excited at its optimum excitation wavelength of 326 nm. Besides, another weak fluorescence emission was also found at 430 nm when the excitation wavelength was at 350 nm, which was attributed to the signal of complex **1**. In comparison to pristine ligand **L1**, the dramatic reduction in emission intensity for **L1** ligand in **1** could be attributed to the fact that **L2** ligand has strong absorption in the infrared region, and the large overlaps between the absorption peak of ligand **L2** and the emission peak of ligand **L1** in complex **1** led to the weak fluorescence emission of complex **1** (Figure 4b). In addition, the azo group is a chromophore that can absorb visible light of a certain wavelength, resulting in **1** having a strong photogenic electron effect. To evaluate the photostability of Zn-MOF, we carried out cycle experiments.

2.4. The Photocurrent Response Performance of Complex **1**

In order to explore the photoelectric performance of complex **1**, we evaluated the photoelectron response performance of this luminescent material. Firstly, the MOF powder-modified indium tin oxide (ITO) glass was chosen to act as the working electrode, and then the working electrode was tested in a sodium sulfate aqueous solution in a standard three-electrode system. Transient photocurrent/time curves for a few of on–off cycles under Xe lamp irradiation reflected that the electrode modified by complex **1** provided a detailed process about their charge separation efficiency levels (Figure 5). The results showed that when the voltage was at 0 V, once the lamp was turned on, the photocurrent value increased quickly to a certain value (1.0 $\mu A \cdot cm^{-2}$), and when the irradiation was canceled, the photocurrent value descended rapidly, and these results were found for three repeats of the experiments (Figure 5b). Besides, when the experiment was performed at −0.5 V, the current value could reach 28.5 $\mu A \cdot cm^{-2}$, and once the lamp was turned on, the photocurrent value increased rapidly to a very high value (34.5 $\mu A \cdot cm^{-2}$) (Figure 5a). These dramatical photocurrent responses evidenced higher separation efficiency levels for photogenerated electron–hole pairs.

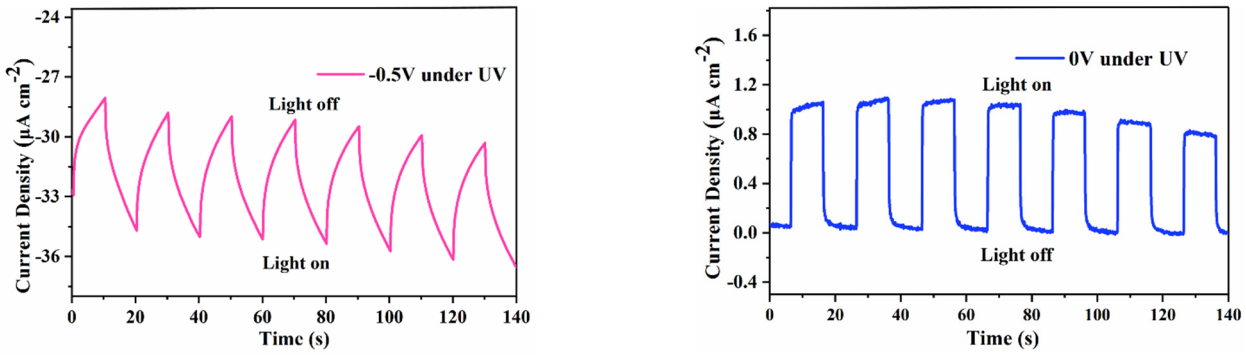

(**a**) (**b**)

Figure 5. Transient photocurrent/time profiles of the bare glassy carbon electrode and **1**, which were coated on the glassy carbon electrode in a KCl electrolyte (0.1 mol·L^{-1}) at a bias of −0.5 V (**a**) and 0.0 V (**b**), with and without light irradiation.

2.5. The Visible-Light-Driven H_2 Production

Based on MOF catalyst **1**, a series of visible-light-driven H_2 generation experiments were executed seriously in a H_2O solution and a mixture solution of DMF and H_2O at the surrounding environment accompanied by Na_2S and Na_2SO_3 as the sacrificial agents. Meanwhile, no additional photosensitizers and co-catalysts were utilized in the process. The study result reflected that under optimized conditions, **1** is highly active for the photocatalytic decomposition of water molecules, generating the production of hydrogen molecules, as well as an average rate of approximately 261 μmol g^{-1} h^{-1} (Figure 6a). Additionally, a new experiment was performed in the absence of **1** under the measured conditions, and the result showed that no detectable hydrogen was found, reflecting that complex **1** played a vital role in the course of photocatalytic hydrogen generation from the water solution. Importantly, the high catalytic efficiency of **1** for decomposing water molecules to generate hydrogen indicated the excellent potential advantage of **1** with no need for additional photosensitizers and cocatalysts in the course of photocatalytic experment. Once the photocatalyzed reaction was finished, the catalyst could be recovered by centrifugation and the complex was washed with ethanol. Then, the recovered catalyst was added into another fresh solution of Na_2S and Na_2SO_3 and illuminated again, and hydrogen could be reproduced with a similar rate as before. Under the same treatment, the catalyst could be used repeatedly for four catalytic cycles (Figure 6b). The PXRD patterns (Figure S2) indicated that **1** could retain its structural stability after the photocatalytic reaction. These results highlight that **1** is an active photocatalyst for visible-light-driven hydrogen evolution. According to the X-ray photoelectron spectra (XPS, Figure S5) of as-synthesized Zn-MOF, the peaks of Zn 2p 3/2 (1022.0 eV) and Zn 2p 1/2 (1045.1 eV) were all sharp and symmetrical, demonstrating that the valence of Zn was +2. In addition, for the Zn-MOF after the photocatalytic reaction, The XPS revealed shifts of 0.4 eV in the Zn 2p3/2 (1021.6 eV) and Zn 2p1/2 (1044.7 eV) peaks toward shift-binding energies (Figure S6). The reason for the lower BE (i.e., less negative orbital energy) of the Zn cationic from the Zn framework can be envisioned, qualitatively, as originating from the less positive charge of the Zn cationic, possibly because the sacrificial agents Na_2S and Na_2SO_3 provided electrons to fill the holes of the Zn cationic in the photocatalytic process.

The apparent quantum yield (AQY) value for Zn-MOF was calculated to be 0.5% by using a Xe lamp equipped with a 420-nm monochromatic light filter and calculated via the following equation:

$$\mathrm{AQY}(\%) = \frac{2 \times \text{ number of } H_2}{\text{number of incident photons}}$$

As we know, under the absence of PS and co-catalysts, the catalyst and sacrificial agent were very important for the production of hydrogen molecules, and changing the individual variables to optimize the photocatalytic activity of **1** is very significative. In

addition, previous literature has shown that the types of another solvent would also affect the activity on producing hydrogen. Therefore, different mixture solutions of DMF/H_2O, MeCN/H_2O, DMAc/H_2O, isopropanol/H_2O, and DMSO/H_2O were discussed. The results revealed that the DMF/H_2O solutions had higher amounts of hydrogen under the same conditions. Moreover, the effect of different ratios of DMF/H_2O on the influence of photocatalytic activity were also carefully explored [46]. Thus, a series of experimental tests were performed carefully and the reaction results acquired in different solvent ratios of DMF/H_2O were displayed and compared (Figure 7). The hydrogen amount produced from these experimental results showed a very similar variation tendency, namely, increasing quickly in the first hours but gradually descending and eventually reaching the maximum. At the same time, we found that different solvent ratios of DMF/H_2O would also affect the photocatalytic activity on the generation of hydrogen in this MOF structure, for example, in DMF/H_2O, when the ratio varied from 2/8 to 3/7 (mL/mL), an obvious enhancement could be found about the average activity from 224 to 291 μmol g^{-1} h^{-1}. Then, when the ratio reached the ratio of 6/4, two distinct hydrogen production rates were found. In the first 8 h, the average rate was very high and the value reached 743 μmol g^{-1} h^{-1}. Then, the rate reduced gradually and the value of average activity was about 396 μmol g^{-1} h^{-1} in the next eight hours. Totally, over 16 h, the experiment performed in DMF/H_2O (v/v, 4/6) produced the most amount of hydrogen (9.1 mmol/g), while the one in DMF/H_2O (v/v, 2/8) produced a lower amount (3.59 mmol). The influence of all these factors on catalytic activity should be ascribed to the effect on light absorption and electron transition during the photocatalytic process.

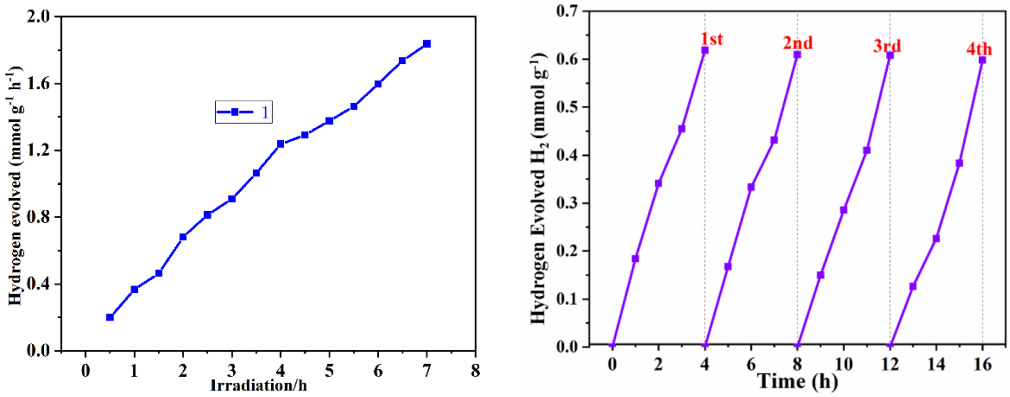

(**a**) (**b**)

Figure 6. (**a**) The rate of hydrogen photogenerated over catalyst **1** (80 mg) in aqueous solutions (100 mL, pH = 11.5) containing Na_2S and Na_2SO_3 under visible light irradiation; (**b**) durability testing for the hydrogen generation of **1**, which was recycled from the reaction solution and used again under the same catalytic condition three times.

2.6. The Photocatalytic Mechanism Study of Hydrogen Production

Careful study revealed that the photocatalytic activity is attributable to the electron transfer between the ligand and the metal [55–67]. Then, the photocatalytic mechanism for hydrogen evolution could be described as follows (Figure 8). The azo unit is a good chromophore and could effectively absorb photoelectrons. Under visible illumination, the azo unit absorbed photoelectrons as well as changed from the ground state to the excited state. Then, the electrons were transferred to Zn clusters. Subsequently, H_2O molecules acquired electrons from the Zn clusters and caused the production of hydrogen. The catalytic circle was fulfilled. Due to the rapid recombination of CB electrons and VB holes in the photocatalytic reaction process, it is difficult to achieve efficient hydrogen production by only using a photocatalyst in pure water. Therefore, the addition of an electron-sacrificing agent can make the irreversible photogenerated hole reaction caused by the valence band, thus accelerating the photogenerated charge separation. Since the

sacrificial agent is always consumed in the reaction process, electron donors need to be continuously added into the system to maintain efficient hydrogen production reaction.

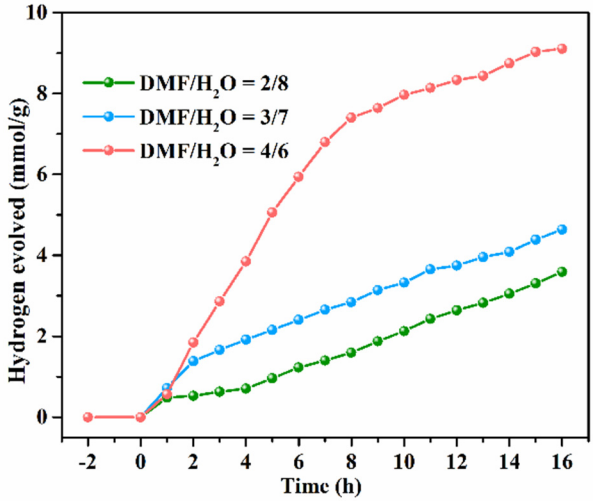

Figure 7. The rate of hydrogen photogenerated over catalyst **1** (80 mg) in different solvent ratio (Total volume: 100 mL, pH = 11.5) containing Na_2S and Na_2SO_3 under visible light irradiation.

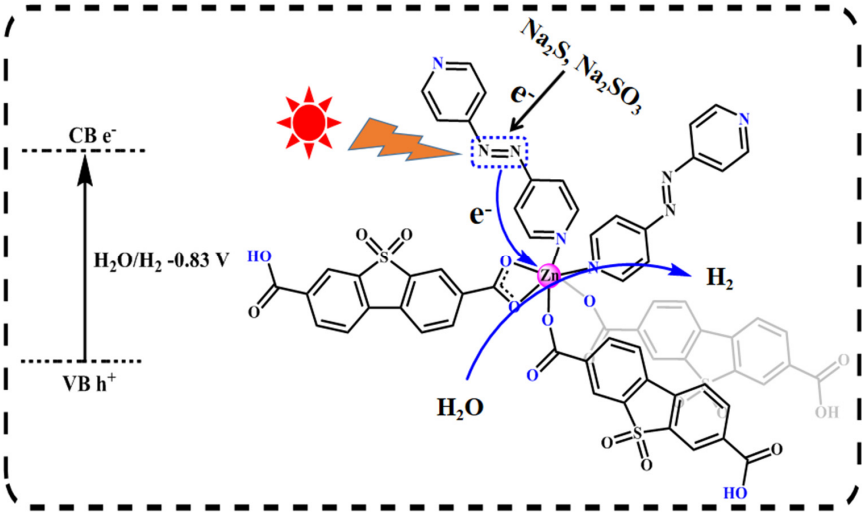

Figure 8. Proposed photocatalytic mechanism of hydrogen evolution for Zn-MOF under visible-light irradiation.

3. Experiment

3.1. Materials and Methods

Analytically pure $Zn(NO_3)_2{\cdot}6H_2O$ was used as metal salt, and two ligands, 4, 4′-bibenzoic acid-2, 2′-sulfone (**L1**) and 4,4′-azopyridine (**L2**), were chosen as connectors. In addition, the Na_2S and Na_2SO_3 were selected as sacrificial agents, and these chemicals were purchased from the chemical company and used without further purification. In addition, the Infrared spectra (IR) measurement was performed on a Nicolet 170SX spectrometer in the range of 4000–400 cm^{-1}. Meanwhile, the Elemental analyses of C, H, and N were executed on a model 2400 Perkin-Elmer analyzer. Besides, a series of PXRD tests reflecting the structural stability were collected on a Bruker D8-ADVANCE X-ray diffractometer with Cu Kα radiation (λ = 1.5418 Å), including a 2θ range of 5°–50° at r.t (room temperature) with a step of 0.02° (2θ) and a counting time of 0.2 s/step. The Thermogravimetric analysis (TGA) experiments were carried out utilizing the SII EXSTAR6000 TG/DTA6300 thermal analyzer from 25 to 800 °C under nitrogen protection as well as a heating rate of 10 °C min^{-1}.

Photoelectric measurements were acquired with a CHI 660E electrochemical workstation, the working area of the working electrode was 1.0 cm^2, and the MOF was modified by ITO. Moreover, the Ag/AgCl was used as a reference electrode and platinum-wire electrode as a counter electrode. All electrochemical tests were performed at room temperature in 0.5 M Na_2SO_4 solution. The leaching test was carried out on the Ultima inductively coupled plasma OES spectrometer (ICP-OES).

General procedure for photocatalytic H_2 evolution. The photocatalytic hydrogen evolution experiments were carried out under a 300 W Xe lamp (PLS-SXE 300C, Beijing PerfectLight Co., Ltd., Beijing, China), and the reactor was a top-irradiation-type Pyrex reaction cell connected to a closed-gas circulation and evacuation system. In a typical experiment, 80 mg of catalyst was dispersed in 100 mL of an aqueous solution containing Na_2S (35.0 mmol, 8.4 g) and Na_2SO_3 (25.0 mmol, 3.15 g) as the sacrificial electron donors. Afterwards, the reaction system was carefully sealed before evacuation for 15 min to completely remove air. Finally, the sealed quartz reactor was irradiated by a Xe lamp equipped with an optical cut off filter ($\lambda > 420$ nm) at a fixed distance (10 cm). During the photocatalytic reaction, the reaction solution was continuously magnetically stirred and kept at 15 °C by a flow of cooling water. The evolved gases were analyzed by gas chromatography with a thermal conductive detector (TCD) and a 5 Å molecular sieve column using N_2 as the carrier gas.

X-ray Photoelectron Spectroscopy (XPS). XPS was conducted using a PHI 5300 spectrometer with a Perkin-Elmer Dual Anode X-ray source operating with magnesium radiation with monochromatic Mg Kα radiation (hν 1253.6 eV) at 13 kV and 250 W and a pass energy of 17.9 eV. A step size of 0.025 eV was used, and 180 sweeps were averaged. Emitted photoelectrons were detected by a hemispherical analyzer and the operating pressure in the sampling chamber was below 1×10^{-7} Torr. The spectral scanning range for nitrogen 1s was 410−390 eV and for cobalt 2p was 765−815 eV. The spectra were calibrated according to the C 1s peak, which is known to occur at 284.6 eV.

3.2. Synthesis of Complex **1**

A mixture of metal salt $Zn(NO_3)_2 \cdot 6H_2O$ (0.2 mmol, 0.058 g), organic connectors H_2bps = 4, 4′-bibenzoic acid-2, 2′-sulfone (0.2 mmol, 0.061 g), and 4,4′-azopyridine (0.1 mmol, 0.018 g), reaction solvents N,N′-dimethylformamide (DMF, 4.5 mL), and H_2O (2.5 mL) was placed in in a 20 mL screw-capped glass jar. Then, the mixture was sealed and heated at 118 °C for 3 days. After that, the reaction system was cooled to 30 °C with about a 6 °C per min cooling rate. After filtration and washing with an excess of N, N′-dimethylformamide (DMF), and ethanol, pink block crystals 1 were collected and dried at room temperature as a pure phase (Yield: 63.5% based on Zn). Anal. Calc. (%) for $C_{24}H_{14}N_4O_6SZn$: C 52.24, H 2.56, N 10.15; found (%): C 52.19, H 2.51, N 10.18. IR (KBr, cm^{-1}): 3067 (w), 2359 (w), 1592 (s), 1562 (s), 1424 (s),1379 (s), 1292 (m), 1175 (m), 1129 (w), 1019 (w), 890 (m), 850 (m), 773 (w), 667 (m), 575 (w), 544 (w), 417 (w).

3.3. X-ray Crystallography

Single-crystal X-ray diffraction data for **1** were acquired at 298 K on an Oxford Diffraction SuperNova area-detector diffractometer by utilizing mirror optics monochromated Mo Kα radiation (λ = 0.71073 Å). CrysAlisPro [68] was utilized for the crystal data collection, general data reduction, and further empirical absorption correction. The crystal structure of **1** was solved by SHELXS-2014 and least-squares refined with SHELXL-2014 [69]. The crystal refinement parameters are provided in Table S2. The X-ray crystallographic coordinated for the structure reported in this study has been deposited at the CCDC under deposition number 2157013. These data can be obtained free of charge from the CCDC via http://www.ccdc.cam.ac.uk/Community/Requestastructure (accessed on 7 March 2022).

4. Conclusions

In summary, a new 3D zinc-based metal-organic framework 1 was built successfully based on a dicarboxylic acid and a dipyridine ligand. The structure and stability of complex **1** was explored in detail by single-crystal X-ray diffraction, IR, elemental analysis, and PXRD test, suggesting the good stability of **1** in different solvents and under distinct pH conditions. Besides, the visible-light-driven hydrogen generation was studied under the illumination of white LED in pure water or a mixture of DMF and H_2O without additional photosensitizers and cocatalysts. The results showed that the visible-light-driven hydrogen evolution ability was enhanced when the ratio of DMF and H_2O varied from 2/8 (mL/mL) to 4/6, and the activity enhanced from 224 to 743 μmol g^{-1} h^{-1}) gradually, reflecting that H_2O content in solvents could affect the activity on producing hydrogen. In addition, the strong absorption of **1** in the UV-vis region with narrow band gap energies (energy: 1.96 eV) reflected good semiconductor performance. The self-sensitized complex **1** opens a new direction of future development of low-cost photocatalysts for efficient and long-term solar fuel production.

Supplementary Materials: The following supporting information can be downloaded at: https://www.mdpi.com/article/10.3390/molecules27061917/s1, Figure S1: PXRD patterns of simulated (Red) and after photocatalytic test in H_2O (Black) of **1**; Figure S2: PXRD patterns of simulated (yellow) and after being immersed samples under H_2O solvent or different mixed solutions of H_2O and DMF of **1**; Figure S3: PXRD patterns of simulated (Black) and after photocatalytic test in a ratio 6:4 of H_2O and DMF (Blue) of **1**; Figure S4: The fluorescence emission spectra before and after the photocatalytic reaction of 1 in aqueous solution; Figure S5: XPS results of **1** (as synthesized), including (a) complete and (b) Zn 2p spectra; Figure S6: XPS results of **1** (after photocatalytic reaction), including (a) complete and (b) Zn 2p spectra; Figure S7: The Tauc's plot (αhv)1/2 vs. (hv), where α is absorbance based on solid-state UV-Vis absorption in Figure 4a. Table S1: Photocatalytic activity of some typical MOF-based photocatalysts for the hydrogen evolution reaction. Table S2: Crystal data and structure refinement for complex **1**.

Author Contributions: T.-T.Z. and T.-T.L.: synthesis of the title complex, formal analysis, IR-related experiment. L.-L.D.: Writing—review and editing. T.C.: completed formal analysis and photocatalytic hydrogen generation experiment. Y.Z. and C.-C.Z.: completed UV-Vis absorption spectra experiment. L.-F.M.: Supervision, writing—review and editing. All authors have read and agreed to the published version of the manuscript.

Funding: This work was supported by the National Natural Science Foundation of China (Grant Nos. 22101108), Project of Central Plains Science and Technology Innovation Leading Talents of Henan Province (No. 204200510001), Natural Science Foundation of Henan Province (No. 212300410209), and the Shanghai Science Technology Committee (19DZ2270100).

Institutional Review Board Statement: Not applicable.

Informed Consent Statement: Not applicable.

Data Availability Statement: Not applicable.

Conflicts of Interest: The authors declare no conflict of interest.

References

1. Hisatomi, T.; Kubota, J.; Domen, K. Recent Advances in Semiconductors for Photocatalytic and Photoelectrochemical Water Splitting. *Chem. Soc. Rev.* **2014**, *43*, 7520–7535. [CrossRef] [PubMed]
2. Ding, C.; Shi, J.; Wang, Z.; Li, C. Photoelectrocatalytic Water Splitting: Significance of Cocatalysts, Electrolyte, and Interfaces. *ACS Catal.* **2017**, *7*, 675–688. [CrossRef]
3. Lianos, P. Review of Recent Trends in Photoelectrocatalytic Conversion of Solar Energy to Electricity and Hydrogen. *Appl. Catal. B Environ.* **2017**, *210*, 235–254. [CrossRef]
4. Gao, C.; Wang, J.; Xu, H.; Xiong, Y. Coordination Chemistry in the Design of Heterogeneous Photocatalysts. *Chem. Soc. Rev.* **2017**, *46*, 2799–2823. [CrossRef] [PubMed]
5. Wang, K.; Li, Y.; Li, J.; Zhang, G. Boosting Interfacial Charge Separation of $Ba_5Nb_4O_{15}$/g-C_3N_4 Photocatalysts by 2D/2D Nano-junction towards Efficient Visible-Light Driven H_2 Generation. *Appl. Catal. B Environ.* **2020**, *263*, 117730. [CrossRef]

6. Wang, S.; Zhu, B.; Liu, M.; Zhang, L.; Yu, J.; Zhou, M. Direct Z-Scheme ZnO/CdS Hierarchical Photocatalyst for Enhanced Photocatalytic H_2 Production Activity. *Appl. Catal. B Environ.* **2019**, *243*, 19–26. [CrossRef]
7. Li, T.; Dang, L.; Zhao, C.; Lv, Z.; Yang, X.; Zhao, Y.; Zhang, S. A self-sensitized Co (II)-MOF for efficient visible-light-driven hydrogen evolution without additional cocatalysts. *J. Solid State Chem.* **2021**, *304*, 122609–122614. [CrossRef]
8. Qin, J.; Xu, P.; Huang, Y.; Xiao, L.; Lu, W.; Yang, X.; Ma, L.; Zang, S. High loading of Mn(II)-metalated porphyrin in MOF for photocatalytic CO_2 reduction in gas–solid condition. *Chem. Commun.* **2021**, *57*, 8468–8471. [CrossRef]
9. Wang, W.; Xu, X.; Zhou, W.; Shao, Z. Recent Progress in Metal-Organic Frameworks for Applications in Electrocatalytic and Photocatalytic Water Splitting. *Adv. Sci.* **2017**, *4*, 1600371. [CrossRef]
10. Zeng, L.; Guo, X.; He, C.; Duan, C. Metal-Organic Frameworks: Versatile Materials for Heterogeneous Photocatalysis. *ACS Catal.* **2016**, *6*, 7935–7947. [CrossRef]
11. Qin, J.-H.; Qin, W.-J.; Xiao, Z.; Yang, J.-K.; Wang, H.-R.; Yang, X.-G.; Li, D.-S.; Ma, L.-F. Efficient energy-transfer-induced high photoelectric conversion in a dye-encapsulated ionic pyrene-based metal–organic framework. *Inorg. Chem.* **2021**, *60*, 18593–18597. [CrossRef] [PubMed]
12. Shi, Y.; Yang, A.; Cao, C.; Zhao, B. Applications of MOFs: Recent Advances in Photocatalytic Hydrogen Production from Water. *Coord. Chem. Rev.* **2019**, *390*, 50–75. [CrossRef]
13. Zhang, T.; Jin, Y.; Shi, Y.; Li, M.; Li, J.; Duan, C. Modulating Photoelectronic Performance of Metal-Organic Frameworks for Premium Photocatalysis. *Coord. Chem. Rev.* **2019**, *380*, 201–229. [CrossRef]
14. Huang, Y.; Liang, J.; Wang, X.; Cao, R. Multifunctional Metal-Organic Framework Catalysts: Synergistic Catalysis and Tandem Reactions. *Chem. Soc. Rev.* **2017**, *46*, 126–157. [CrossRef] [PubMed]
15. Xu, Z.; Xiong, X.; Xiong, J.; Krishna, R.; Li, L.; Fan, Y.; Luo, F.; Chen, B. A robust Th-azole framework for highly efficient purification of C_2H_4 from a $C_2H_4/C_2H_2/C_2H_6$ mixture. *Nat. Commun.* **2020**, *11*, 3163. [CrossRef] [PubMed]
16. Luo, F.; Yang, C.; Dang, L.; Krishna, R.; Zhou, W.; Wu, H.; Dong, X.; Han, Y. UTSA-74: A MOF-74 isomer with two accessible binding sites per metal center for highly selective gas separation. *J. Am. Chem. Soc.* **2016**, *138*, 5678–5684. [CrossRef] [PubMed]
17. Li, J.; Kuppler, R.; Zhou, H. Selective gas adsorption and separation in metal-organic frameworks. *Chem. Soc. Rev.* **2009**, *38*, 1477–1504. [CrossRef]
18. Yang, G.; Hou, L.; Ma, L.; Wang, Y. Investigation on the prime factors influencing the formation of entangled metal–organic frameworks. *CrystEngComm* **2013**, *15*, 2561–2578. [CrossRef]
19. Wu, X.; Fu, H.; Han, M.; Zhou, L.; Ma, L. Tetraphenylethylene Immobilized Metal–Organic Frameworks: Highly Sensitive Fluorescent Sensor for the Detection of $Cr_2O_7^{2-}$ and Nitroaromatic Explosives. *Cryst. Growth Des.* **2017**, *17*, 6041–6048. [CrossRef]
20. Han, M.; Duan, Y.; Li, D.; Xu, G.; Wu, Y.; Zhao, J. A series of divalent metal coordination polymers based on isomeric tetracarboxylic acids: Synthesis, structures and magnetic properties. *Dalton Trans.* **2014**, *43*, 17519–17527. [CrossRef] [PubMed]
21. Ma, L.; Han, M.; Qin, J.; Wang, L.; Wang, L.; Du, M. Mn-II coordination polymers based on Bi-, Tri- and tetranuclear and polymeric chain building units: Crystal structures and magnetic properties. *Inorg. Chem.* **2012**, *51*, 9431–9442. [CrossRef] [PubMed]
22. Liu, J.; Luo, Z.; Pan, Y.; Singh, A.; Trivedi, M.; Kumar, A. Recent developments in luminescent coordination polymers: Designing strategies, sensing application and theoretical evidences. *Coord. Chem. Rev.* **2020**, *406*, 213145. [CrossRef]
23. Chang, X.H.; Qin, J.H.; Han, M.L.; Ma, L.F.; Wang, L.Y. Exploring the structural diversities and magnetic properties of copper (II) and manganese (II) complexes based on 5-methoxyisophthalate and flexible bis (imidazole) ligands. *CrystEngComm* **2014**, *16*, 870–882. [CrossRef]
24. Meng, X.; Wang, H.; Song, S.; Zhang, H. Proton-Conducting Crystalline Porous Materials. *Chem. Soc. Rev.* **2017**, *46*, 464–480. [CrossRef] [PubMed]
25. Lu, K.; Aung, T.; Guo, N.; Weichselbaum, R.; Lin, W. Nanoscale Metal-Organic Frameworks for Therapeutic, Imaging, and Sensing Applications. *Adv. Mater.* **2018**, *30*, 1707634. [CrossRef]
26. Chang, X.H.; Zhao, Y.; Han, M.L.; Ma, L.F.; Wang, L.Y. Five Cd (II) coordination polymers based on 2,3′,5,5′-biphenyltetracarboxylic acid and N-donor coligands: Syntheses, structures and fluorescent properties. *CrystEngComm* **2014**, *16*, 6417–6424. [CrossRef]
27. Chang, X.H.; Qin, W.J.; Zhang, X.Y.; Jin, X.; Yang, X.G.; Dou, C.X.; Ma, L.F. Angle-Dependent Polarized Emission and Photoelectron Performance of Dye-Encapsulated Metal-Organic Framework. *Inorg. Chem.* **2021**, *60*, 10109–10113. [CrossRef]
28. Sutherland, B.; Hoogland, S.; Adachi, M.; Kanjanaboos, P.; Wong, C.; McDowell, J.; Xu, J.; Voznyy, O.; Ning, Z.; Houtepen, A.; et al. Perovskite Thin Films via Atomic Layer Deposition. *Adv. Mater.* **2015**, *27*, 53–58. [CrossRef]
29. Yang, X.; Zhai, Z.; Lu, X.; Qin, J.; Li, F.; Ma, L. Hexanuclear Zn (II)-Induced Dense π-Stacking in a Metal–Organic Framework Featuring Long-Lasting Room Temperature Phosphorescence. *Inorg. Chem.* **2020**, *59*, 10395–10399. [CrossRef]
30. Yang, X.; Lu, X.; Zhai, Z.; Qin, J.; Chang, X.; Han, M.; Li, F.; Ma, L. π-Type halogen bonding enhanced the long-lasting room temperature phosphorescence of Zn (II) coordination polymers for photoelectron response applications. *Inorg. Chem. Front.* **2020**, *7*, 2224–2230. [CrossRef]
31. Chang, X.H.; Ling, X.L.; Lu, X.M.; Yang, X.G.; Li, F.F.; Guo, Y.M. Near-infrared phosphorescence emission of three-fold interpenetrated MOF based on 1,4-bis (imidazole-1-ylmethyl) benzene: Syntheses, structure and photoelectron performance. *J. Solid State Chem.* **2020**, *292*, 121694. [CrossRef]
32. Qin, J.; Zhang, H.; Sun, P.; Huang, Y.; Shen, Q.; Yang, X.; Ma, L. Ionic liquid induced highly dense assembly of porphyrin in MOF nanosheets for photodynamic therapy. *Dalton Trans.* **2020**, *49*, 17772–17778. [CrossRef]

33. Zhao, Y.; Yang, X.; Lu, X.; Yang, C.; Fan, N.; Yang, Z.; Wang, L.; Ma, L. {Zn6} cluster based metal-organic framework with enhanced room-temperature phosphorescence and optoelectronic performances. *Inorg Chem.* **2019**, *58*, 6215–6221. [CrossRef] [PubMed]
34. Dang, L.; Li, T.; Cui, Z.; Sui, D.; Ma, L.; Jin, G. Selective construction and stability studies of molecular trefoil knot and Solomon link. *Dalton Trans.* **2021**, *50*, 16984–16989. [CrossRef] [PubMed]
35. Zhao, Y.; Wang, L.; Fan, N.; Han, M.; Yang, G.; Ma, L. Porous Zn(II)-based metal–organic frameworks decorated with carboxylate groups exhibiting high gas adsorption and separation of organic dyes. *Cryst. Growth & Des.* **2018**, *18*, 7114–7121.
36. Dang, L.; Li, T.; Zhao, C.; Zhang, T.; Ye, X.; Sun, X.; Wang, H.; Ma, L. Supramolecular Rh6 catalytic system promoting directed [4 + 4] cycloaddition reaction of anthracene under UV irradiation. *J. Solid State Chem.* **2022**, *306*, 122785–122792. [CrossRef]
37. Meyer, K.; Ranocchiari, M.; van Bokhoven, J.A. Metal organic frameworks for photo-catalytic water splitting. *Energy Environ. Sci.* **2015**, *8*, 1923–1937. [CrossRef]
38. Lan, M.; Guo, R.M.; Dou, Y.B.; Zhou, J.; Zhou, A.; Li, J.R. Fabrication of porous Pt-doping heterojunctions by using bimetallic MOF template for photocatalytic hydrogen generation. *Nano Energy.* **2017**, *33*, 238–246. [CrossRef]
39. Liao, W.-M.; Zhang, J.-H.; Wang, Z.; Yin, S.-Y.; Pan, M.; Wang, H.-P.; Su, C.-Y. Post-synthetic exchange (PSE) of UiO-67 frameworks by Ru/Rh half-sandwich units for visible-light-driven H_2 evolution and CO_2 reduction. *J. Mater. Chem. A* **2018**, *6*, 11337–11345. [CrossRef]
40. Dhakshinamoorthy, A.; Li, Z.H.; Garcia, H. Catalysis and photocatalysis by metal organic frameworks. *Chem. Soc. Rev.* **2018**, *47*, 8134–8172. [CrossRef] [PubMed]
41. Zhen, W.L.; Ma, J.T.; Lu, G.X. Small-sized Ni (1 1 1) particles in metal-organic frameworks with low over-potential for visible photocatalytic hydrogen generation. *Appl. Catal. B Environ.* **2016**, *190*, 12–25. [CrossRef]
42. Nasalevich, M.; Becker, R.; Ramos-Fernandez, E.; Castellanos, S.; Veber, S.; Fedin, M.; Kapteijn, F.; Reek, J.; van der Vlugt, J.; Gascon, J. Co@NH_2-MIL-125 (Ti): Cobaloxime-derived metal-organic framework-based composite for light-driven H_2 production. *Energy Environ. Sci.* **2015**, *8*, 364–375. [CrossRef]
43. Wu, P.; Guo, X.; Cheng, L.; He, C.; Wang, J.; Duan, C. Photoactive Metal-Organic Framework and Its Film for Light-Driven Hydrogen Production and Carbon Dioxide Reduction. *Inorg. Chem.* **2016**, *55*, 8153–8159. [CrossRef] [PubMed]
44. Feng, Y.; Chen, C.; Liu, Z.; Fei, B.; Lin, P.; Li, Q.; Sun, S.; Du, S. Application of a Ni mercaptopyrimidine MOF as highly efficient catalyst for sunlight-driven hydrogen generation. *J. Mater. Chem. A* **2015**, *3*, 7163–7169. [CrossRef]
45. Liao, W.; Zhang, J.; Hou, Y.; Wang, H.; Pan, M. Visible-light-driven CO_2 photo-catalytic reduction of Ru (II) and Ir (III) coordination complexes. *Inorg. Chem. Commun.* **2016**, *73*, 80–89. [CrossRef]
46. Liao, W.; Zhang, J.; Wang, Z.; Lu, Y.; Yin, S.; Wang, H.; Fan, Y.; Pan, M.; Su, C. Semiconductive Amine-Functionalized Co (II)-MOF for Visible-Light-Driven Hydrogen Evolution and CO_2 Reduction. *Inorg. Chem.* **2018**, *57*, 11436–11442. [CrossRef] [PubMed]
47. Shi, D.; Zheng, R.; Sun, M.; Cao, X.; Sun, C.; Cui, C.; Liu, C.; Zhao, J.; Du, M. Semiconductive Copper (I)-Organic Frameworks for Efficient Light-Driven Hydrogen Generation Without Additional Photosensitizers and Cocatalysts. *Angew. Chem. Int. Ed.* **2017**, *56*, 14637–14641. [CrossRef] [PubMed]
48. Luo. M., J.; Wang. Y., L.; Huang, T.B.; Su, T.; Fu, D.H.; Yue, S.T.; Zeng, H.P. Application of an Mn-MOF as a highly efficient catalyst for sunlight-driven hydrogen generation. *Phase Transitions.* **2018**, *91*, 1179–1187. [CrossRef]
49. Wen, M.; Mori, K.; Kamegawa, T.; Yamashita, H. Amine-functionalized MIL-101 (Cr) with imbedded platinum nanoparticles as a durable photocatalyst for hydrogen production from water. *Chem. Commun.* **2014**, *50*, 11645–11648. [CrossRef]
50. Zhang, S.; Li, L.; Zhao, S.; Sun, Z.; Luo, J. Construction of interpenetrated ruthenium metal-organic frameworks as stable photocatalysts for CO_2 reduction. *Inorg. Chem.* **2015**, *54*, 8375–8379. [CrossRef]
51. Yang, G.; Che, X.; Hou, S.; Cao, C.; Zhao, B. Photocatalytic Hydrogen Evolution Based on Cobalt–Organic Framework with High Water Vapor Adsorption. *Inorg. Chem.* **2021**, *60*, 1922–1929. [CrossRef] [PubMed]
52. Qin, J.; Jia, Y.; Li, H.; Zhao, B.; Wu, D.; Zang, S.; Hou, H.; Fan, Y. Conversion from a Heterochiral [2 + 2] Coaxially Nested Double-Helical Column to a Cationic Spiral Staircase Stimulated by an Ionic Liquid Anion. *Inorg. Chem.* **2014**, *53*, 685–687. [CrossRef] [PubMed]
53. Xu, W.; Ma, L.; Ke, F.; Peng, F.; Xu, G.; Shen, Y.; Zhu, J.; Qiu, L.; Yuan, Y. Metal–organic frameworks MIL-88A hexagonal microrods as a new photocatalyst for efficient decolorization of methylene blue dye. *Dalton Trans.* **2014**, *43*, 3792–3798. [CrossRef] [PubMed]
54. Liu, S.; Zhang, C.; Sun, Y.; Chen, Q.; He, L.; Zhang, K.; Zhang, J.; Liu, B.; Chen, L. Design of metal-organic framework-based photocatalysts for hydrogen generation. *Coord. Chem. Rev.* **2020**, *413*, 213266–213283. [CrossRef]
55. Toyao, T.; Saito, M.; Horiuchi, Y.; Mochizuki, K.; Iwata, M.; Higashimura, H.; Matsuoka, M. Efficient hydrogen production and photocatalytic reduction of nitrobenzene over a visible-light-responsive metal–organic framework photocatalyst. *Catal. Sci. Technol.* **2013**, *3*, 2092–2097. [CrossRef]
56. Zhou, T.; Du, Y.; Borgna, A.; Hong, J.; Wang, Y.; Han, J.; Zhang, W.; Xu, R. Post-synthesis modification of a metal–organic framework to construct a bifunctional photocatalyst for hydrogen production. *Energy Environ. Sci.* **2013**, *6*, 3229–3234. [CrossRef]
57. Lin, R.; Shen, L.; Ren, Z.; Wu, W.; Tan, Y.; Fu, H.; Zhang, J.; Wu, L. Enhanced photocatalytic hydrogen production activity via dual modification of MOF and reduced graphene oxide on CdS. *Chem. Commun.* **2014**, *50*, 8533–8535. [CrossRef]
58. Yuan, Y.; Yin, L.; Cao, S.; Xu, G.; Li, C.; Xue, C. Improving photocatalytic hydrogen production of metal–organic framework UiO-66 octahedrons by dye-sensitization. *Appl. Catal. B Environ.* **2015**, *572*, 168–169. [CrossRef]

59. Toyao, T.; Saito, M.; Dohshi, S.; Mochizuki, K.; Iwata, M.; Higashimura, H.; Horiuchi, Y.; Matsuoka, Y. Development of a Ru complex-incorporated MOF photocatalyst for hydrogen production under visible-light irradiation. *Chem. Commun.* **2014**, *50*, 6779–6781. [CrossRef]
60. He, J.; Wang, J.; Chen, Y.; Zhang, J.; Duan, D.; Wang, Y.; Yan, Z. A dye-sensitized Pt@UiO-66(Zr) metal–organic framework for visible-light photocatalytic hydrogen production. *Chem. Commun.* **2014**, *50*, 7063–7066. [CrossRef]
61. Zhao, X.; Feng, J.; Liu, J.; Shi, W.; Yang, G.; Wang, G.; Cheng, P. An Efficient, Visible-Light-Driven, Hydrogen Evolution Catalyst NiS/ZnxCd1-xS Nanocrystal Derived from a Metal-Organic Framework. *Angew. Chem. Int. Ed.* **2018**, *26*, 9790–9794. [CrossRef] [PubMed]
62. Li, D.; Yu, S.; Jiang, H. From UV to Near-Infrared Light-Responsive Metal–Organic Framework Composites: Plasmon and Upconversion Enhanced Photocatalysis. *Adv. Mater.* **2018**, *30*, 1707377. [CrossRef] [PubMed]
63. Fang, X.; Shang, Q.; Wang, Y.; Jiao, L.; Yao, T.; Li, Y.; Zhang, Q.; Luo, Y.; Jiang, H. Single Pt Atoms Confined into a Metal–Organic Framework for Efficient Photocatalysis. *Adv. Mater.* **2018**, *30*, 1705112. [CrossRef]
64. Li, Z.; Xiao, J.; Jiang, H. Encapsulating a Co(II) Molecular Photocatalyst in Metal−Organic Framework for Visible-Light-Driven H_2 Production: Boosting Catalytic Efficiency via Spatial Charge Separation. *ACS Catal.* **2016**, *6*, 5359–5365. [CrossRef]
65. Lan, G.; Zhu, Y.; Veroneau, S.; Xu, Z.; Micheroni, D.; Lin, W. Electron Injection from Photoexcited Metal−Organic Framework Ligands to Ru_2 Secondary Building Units for Visible-Light-Driven Hydrogen Evolution. *J. Am. Chem. Soc.* **2018**, *140*, 5326–5329. [CrossRef] [PubMed]
66. Yuan, S.; Qin, J.; Xu, H.; Su, J.; Rossi, D.; Chen, Y.; Zhang, L.; Lollar, C.; Wang, Q.; Jiang, H.; et al. $[Ti_8Zr_2O_{12}(COO)_{16}]$ Cluster: An Ideal Inorganic Building Unit for Photoactive Metal−Organic Frameworks. *ACS Cent. Sci.* **2018**, *4*, 105–111. [CrossRef]
67. Xiao, J.D.; Shang, Q.; Xiong, Y.; Zhang, Q.; Luo, Y.; Yu, S.H.; Jiang, H.L. Boosting Photocatalytic Hydrogen Production of a Metal−Organic Framework Decorated with Platinum Nanoparticles: The Platinum Location Matters. *Angew. Chem. Int. Ed.* **2016**, *55*, 9389–9393. [CrossRef]
68. Sheldrick, G.M. Phase annealing in SHELX-90: Direct methods for larger structures. *Acta Crystallogr. Sect. A Found. Crystallogr.* **1990**, *46*, 467–473. [CrossRef]
69. Sheldrick, G.M. A short history of SHELX. *Acta Crystallogr.* **2008**, *64*, 112–122. [CrossRef]